Reconstruction of 3D Ozone Fields Using POAM III During SOLVE

C.E. Randall[1], J.D. Lumpe[2], R.M. Bevilacqua[3], K.W. Hoppel[3], M.D. Fromm[2], R.J. Salawitch[4], W.H. Swartz[5,6], S.A. Lloyd[5], E. Kyro[7], P. von der Gathen[8], H. Claude[9], J. Davies[10], H. DeBacker[11], H. Dier[12], M.J. Molyneux[13], and J. Sancho[14]

[1] Laboratory for Atmospheric and Space Physics, University of Colorado, Boulder, CO 80309-0392. Tel: 303-492-8208; Fax: 303-492-6946; email: cora.randall@lasp.colorado.edu. [2] Computational Physics, Inc., 8001 Braddock Road, Suite 210, Springfield, VA 22151. Tel: 703-764-7501; Fax: 703-764-7500; email: lumpe@cpi.com; fromm@poamb.nrl.navy.mil. [3] Naval Research Laboratory, Code 7220, Bldg. 2, 4555 Overlook Ave., SW, Washington, DC 20375-5320. Tel: 202-767-0768; Fax: 202-767-7885; email: bevilacqua@nrl.navy.mil; karl.hoppel@nrl.navy.mil. [4] Jet Propulsion Laboratory, MS 183-301, 4800 Oak Grove Dr., Pasadena, CA 91109. Tel: 818-354-0442; Fax: 818-354-5148; email: rjs@caesar.jpl.nasa.gov. [5] The Johns Hopkins University Applied Physics Laboratory. Tel: 240-228-8462; email: bill.swartz@jhuapl.edu; steven_lloyd@jhuapl.edu. [6] Department of Chemistry and Biochemistry, University of Maryland, College Park, MD 20742. [7] FMI Sodankylä observatory, Tähteläntie 71, FIN-99600 Sodankylä, Finland. Tel: +358-16-610 072; fax: +358-16-610 105; email: esko.kyro@fmi.fi. [8]Alfred Wegener Institute for Polar and Marine Research, Research Site Potsdam, Telegrafenberg A43, D-14473 Potsdam. Tel: +49-331-288-2128; Fax: +49-331-288-2178; email: gathen@awi-potsdam.de. [9]Hohenpeissenberg Observatory, Deutscher Wetterdienst, Albin-Schwaiger-Weg 10, 82383, Hohenpeissenberg, Germany. email: hans.claude@dwd.de. [10]jonathan.davies@ec.gc.ca. [11]Royal Meteorological Institute of Belgium, Ringlaan 3, B-1180 Brussels, Belgium. Tel: +32-2-3730594; Fax: +32-2-3751259; email: hugo.debacker@oma.be. [12]DWD Meteorological Observatory Lindenberg, Am Observatorium 12, 15864 Lindenberg. Tel: +49-33677-60231; Fax: +49-33677-60280; email: horst.dier@dwd.de. [13]Met Office, Beaufort Park, Easthampstead, Wokingham, Berks, RG40 3DN, United Kingdom; email: mjmolyneux@meto.gov.uk. [14]Izana Atmospheric Observatory, La Marina, 20, PO Box 880, Santa Cruz de Tenerife, Spain, 38071; email: jsancho@inm.es.

Abstract
In this paper, we demonstrate the utility of the Polar Ozone and Aerosol Measurement (POAM) III data for providing semi-global three-dimensional ozone fields during the SAGE III Ozone Loss and Validation Experiment (SOLVE) winter. As a solar occultation instrument, POAM III measurements were limited to latitudes of 63°N to 68°N during the SOLVE campaign, but covered a wide range of potential vorticity. Using established mapping techniques, we have used the relation between potential vorticity and ozone measured by POAM III to calculate three-dimensional ozone mixing ratio fields throughout the northern hemisphere on a daily basis during the 1999-2000 winter. To validate the results, we have extensively compared profiles obtained from ozonesondes and the Halogen Occultation Experiment to the proxy O_3 interpolated horizontally and vertically to the correlative measurement locations. On average, the proxy O_3 agrees with the correlative observations to better than ~5%, at potential temperatures below about 900 K and latitudes above about 30°N, demonstrating the reliability of the reconstructed O_3 fields in these regions. We discuss the application of the POAM proxy ozone profiles for calculating photolysis rates along the ER-2 and DC-8 flight tracks during the SOLVE campaign, and present a qualitative picture of the evolution of polar stratospheric ozone throughout the winter.

1. Introduction

The SAGE III Ozone Loss and Validation Experiment (SOLVE) campaign was designed to investigate the processes causing O_3 loss at high northern latitudes, and to provide correlative data for validating the Stratospheric Aerosol and Gas Experiment (SAGE) III. One of the goals of SOLVE was to optimize the inference of O_3 loss from satellite observations, for those years when dedicated ground, balloon and/or aircraft campaigns are not feasible. Although the launch of SAGE III was unfortunately delayed, the Polar Ozone and Aerosol Measurement (POAM) III instrument, a satellite-based solar occultation instrument with latitude coverage similar to the planned SAGE III measurements, was (and still is) operational. During the SOLVE campaign, POAM III provided daily stratospheric profiles of ozone, water vapor, nitrogen dioxide and aerosol extinction in the northern hemisphere (NH) from 63°N to 68°N with about 1-km vertical resolution. These measurements are being used to investigate the polar processes responsible for O_3 loss during the 1999-2000 NH winter [e.g., *Hoppel et al*., 2001; *Bevilacqua et al*., 2001; both in this issue].

It is now well established that the 1999-2000 NH polar vortex was unusually cold, with temperatures often below the threshold for forming Polar Stratospheric Clouds (PSCs) [*Manney and Sabutis*, 2000]. O_3 decreases inside the polar vortex of 0.04±0.01 ppmv/day were observed in Microwave Limb Sounder (MLS) data from early February [*Santee et al*., 2000], and O_3 chemical loss of more than 70% by the end of March has been inferred from ozonesonde data at Ny Ålesund, Spitsbergen (79°N, 12°E) [*Sinnhuber et al*., 2000]. Nevertheless, the precise mechanisms controlling the magnitude of the O_3 loss have yet to be elucidated in detail. Ideally, a campaign such as SOLVE would be supported by global satellite measurements, with the ground-based, balloon and aircraft measurements providing detailed but localized information, and the satellite providing measurements to place this information into a more global context. Although the Total Ozone Mapping Spectrometer (TOMS) instrument provides an excellent near-global map of column O_3, vertically resolved measurements are often preferable for mechanistic studies. Unfortunately, no instrument capable of providing global O_3 profiles with

high vertical resolution was operational throughout the SOLVE campaign (although the MLS was operational for nine days in February and March [*Santee et al*., 2000]).

In an effort to improve this situation, we have reconstructed daily, semi-global (NH only), vertically resolved O_3 fields from the POAM data. The technique by which this was accomplished, which we refer to as potential vorticity (PV) mapping, was established more than a decade ago for use with LIMS [*Butchart and Remsberg,* 1986] and ER-2 [*Schoeberl et al*., 1989] data. This technique makes it possible, under certain conditions, to calculate mixing ratios over a much wider range of geographic locations than were actually observed. In this paper we describe the PV mapping technique as applied to the POAM III data, validate the results, and show how these results are useful for the SOLVE objectives.

The premise behind the PV mapping technique is that PV is a conserved quantity during adiabatic transport, so it is often used as a tracer of atmospheric motions. Since O_3 in the winter stratosphere is dynamically controlled, a single, well-defined relationship defines its correlation with PV across the polar vortex anywhere on a given potential temperature (θ) surface at any given point in time [e.g., *Leovy et al*., 1985, *Allaart et al*., 1993]. If this relationship is determined by measuring O_3 over a sufficient range of PV/θ space, it can thus be used to derive O_3 mixing ratios at geographic locations outside the actual measurement field, as long as the PV and θ values at those locations are known. The technique has been incorporated into studies of vortex processes in both hemispheres [*Schoeberl et al.*, 1989; *Lait et al*., 1990; *Manney et al*., 1998; 1999], and the underlying concepts have been used to improve satellite data intercomparisons [*Manney et al*., 2001; *Redaelli et al*., 1994]. This paper describes its first application with POAM III O_3 data. POAM III routinely measured O_3 profiles over a wide range of PV during the SOLVE campaign (see section 2). Taking advantage of the PV analyses from the Met Office (UKMO) [*Swinbank and O'Neill*, 1994], we were able to reconstruct O_3 profiles on the NH UKMO grid, as described in section 3. We evaluated the NH gridded O_3 "proxy" product by interpolating the profiles vertically and horizontally to the locations of correlative measurements, to which we compared the proxy profiles. These comparisons are described in section 4. The initial motivation for performing and validating the PV-mapping with POAM III data during SOLVE was to derive O_3 profiles above the SOLVE aircraft measurements. These profiles could then be used to determine solar flux transmissions for theoretical calculations of photolysis reaction rates. This application of the proxy O_3 data is the subject of section 5.

2. POAM III Data

Each day, approximately fifteen POAM observations, separated by ~25° in longitude, are made around a circle of approximately constant latitude in the northern hemisphere (NH) at local sunset. The average latitude of the observations on each day from 1 November 1999 through 30 April 2000 is shown in Figure 1. At each measurement location, POAM measures profiles of O_3 (~10-60 km), aerosol extinction at five wavelengths from 353 nm to 1020 nm (~10-30 km), NO_2 (~20-40 km), and H_2O (~10-45 km). In this paper, we focus on the version 3.0 POAM III O_3 data. Preliminary validation of an earlier version of POAM III O_3 was described by *Lucke et al*. [1999]. More recent analyses with version 3.0 have been completed by *Lumpe et al*. [2001, this issue] and *Rusch et al*. (Validation of POAM III O_3: Comparison to ozonesonde and satellite data, submitted to *J. Geophys. Res.*, 2001). These show that on average, POAM III O_3 profiles in the NH agree to better than 10% with correlative observations from 12 to 60 km.

Because the vortex is often displaced from the pole in the NH, POAM III makes measurements at a wide range of equivalent latitudes [*Butchart and Remsberg, 1986*] on a daily basis during the winter, even though the geographic latitude is essentially constant on a given day. For example, Plate 1 shows the PV on the 500 K potential temperature surface corresponding to every POAM measurement in the NH from 1 November 1999 through 30 April 2000. For this figure and elsewhere in the paper, we use UKMO PV analyses interpolated in time and space to the POAM measurement locations when necessary. The inner and outer vortex edge boundaries, as defined by *Nash et al*. [1996], are denoted in the plot. From late December through mid-March, POAM sampled in the vortex core, on the vortex edge, and outside the vortex on a near-daily basis. It is this characteristic of the POAM measurements that allows the analysis described below.

To illustrate how O_3 changes with PV, a contour plot of the O_3 field generated from measurements obtained by POAM over a 3-day period from 24-26 December 1999 is given in Plate 2. Maps such as this were provided to SOLVE campaign participants on a daily basis throughout the winter. At this particular time and latitude, measurement locations at longitudes of about 330°E to 60°E were inside the vortex (in-V), with longitudes near 180° well outside the vortex (out-V), and longitudes near 120°E and 300°E on the edge of the vortex (edge-V). This is quite typical for the vortex structure and location in the NH. Since O_3 is in dynamical control at this time and latitude, mixing ratios follow the vortex structure. At all altitudes above about 500 K, O_3 mixing ratios are significantly higher outside the vortex than inside; this results largely from transport of O_3-rich air from lower latitudes to the polar region outside the vortex [*Randall et al*., 1995]. Inside the vortex, air parcels cannot mix as freely with the lower latitude air, so mixing ratios remain lower than outside the vortex. Near 450 K, where the vertical gradient in the O_3 profile is larger than at the higher altitudes, O_3 mixing ratios inside the vortex are slightly higher than outside. This is due to enhanced diabatic descent inside the vortex. Because O_3 mixing ratios increase with altitude here, air parcels descending inside the vortex to 450 K increase the O_3 mixing ratios to values above those outside the vortex, where descent occurs less rapidly and with more horizontal mixing [e.g., *Randall et al*., 1995; Manney *et al*., 1995a, and references therein].

Whereas Plate 2 illustrates the O_3 variation with respect to the vortex that was observed in late December, Plate 3 presents the temporal variation in O_3 that was observed at different locations with respect to the vortex over the course of the winter. This figure shows the daily average POAM III O_3 mixing ratios segregated according to position with respect to the vortex (e.g., inside, outside, or on the edge) using the *Nash et al*. [1996] vortex definition. Although these observations were all acquired within the fairly narrow latitude band depicted in Figure 1, they illustrate some interesting features of the changes in vortex distribution of O_3 during the winter at these latitudes. For instance, at 550 K and 600 K, in-V mixing ratios are persistently lower than out-V mixing ratios, for the reasons stated above relating to poleward transport of high O_3 mixing ratio air from lower latitudes. At 450 K in December, in-V O_3 is more than 50% higher than out-V O_3. Again, this was explained above, and results from enhanced diabatic descent inside the vortex. However, in-V O_3 mixing ratios at 450 K begin to decline steeply by mid-February, so that by early March they are as low as out-V mixing ratios. This is the signature of chemical O_3 loss, and is discussed in more detail by *Hoppel et al*. [2001, this issue]. By early March, even edge-V O_3 is declining at 450 K. Similar declines in in-V and edge-V O_3 are also

evident at 500 K. Another interesting feature is that until about mid-January, edge-V mixing ratios at 500 K are higher than both in-V and out-V. We believe that this can be explained primarily by a variation across the edge of the vortex in the O_3 profile vertical gradient near 500 K. Examination of POAM III profiles in October and November reveals that edge-V and out-V O_3 mixing ratio profiles exhibited a steep gradient from 400 to 600 K. Enhanced diabatic descent on the edge of the vortex would have resulted in higher edge-V O_3 than out-V, just as at 450 K. However, whereas in-V O_3 mixing ratios followed a similarly steep gradient from 400 to 500 K, they were roughly constant near 3.0 ppmv or less above about 500 K. Thus, enhanced diabatic descent inside the vortex produced little change in the in-V O_3 mixing ratios at this time, resulting in edge-V O_3 mixing ratios that were higher than both in-V and out-V. There may also be a contribution from faster diabatic descent along the edge of the vortex compared to inside. Reverse trajectory calculations performed elsewhere (G. Manney, *private communication*, 2001) showed that air parcels at 500 K on 5 January would have descended ~10 K further on the edge of the vortex than inside during the preceding 40 days .

3. Method

As mentioned above, the fact that PV is conserved during adiabatic transport allows us to use it to follow the motion of tracers (such as O_3 under many conditions) on isentropic surfaces. This concept can be applied to approximate O_3 at geographic locations distant from actual measurements, as long as the measurements themselves adequately constrain the relationship between PV and O_3, and the PV values at the remote locations are well known [e.g., *Schoeberl et al*., 1989]. As shown above, POAM III measurements span a wide range of PV values daily throughout the NH winter, and clearly document variations in O_3 expected from the changing PV. For every day during the SOLVE campaign, we thus calculated an analytic (quadratic) expression relating PV to O_3 using the POAM III O_3 profiles and the UKMO PV values interpolated in time and space to the POAM measurement locations. In practice, we actually used O_3 and PV data corresponding to the 7-day interval centered on the day of interest. We found by trial and error that this interval length corresponded to the optimum balance for defining the PV/O_3 relation. Including more days introduces error due to varying PV/O_3 correlations, particularly in times of rapid vortex evolution. Including fewer days results in poorer statistics – in general the quadratic fits in these cases were qualitatively similar to the 7-day analyses, but suffered from more noise. For each day during the SOLVE winter, we then applied this relation to the daily 12:00 UT NH UKMO PV field to generate proxy O_3 mixing ratios on the same latitude/longitude grids as the UKMO data (for this work these grids spanned the NH in 2.5-degree increments in latitude and 3.75-degree increments in longitude).

Our method is illustrated in Plate 4 for 1 January 2000 at 650 K. Plate 4a shows the POAM III O_3 mixing ratios from 29 December through 4 January plotted against the UKMO PV interpolated to the POAM III measurement locations on the 650 K surface. For this altitude and time, high PV values correspond to the lowest values of O_3, and low PV values to the highest values of O_3, since O_3 outside the vortex is higher than inside, as discussed above. Superimposed on the data is a quadratic fit. We calculated a proxy O_3 field for this day by multiplying the 650 K UKMO PV grid for January 1 by the quadratic coefficients defining the fit in Plate 4a. Plate 4b shows a contour map of the UKMO PV, clearly depicting the vortex as having an oval shape with its long axis oriented along 90°E-270°E longitude, and its center displaced from the pole toward Greenland and Scandinavia. Over the 7-day period from 29

December to 4 January the POAM measurements spanned the latitude circle near 63°, in fairly regular longitude intervals of about five degrees. The measurements occurred well outside and inside the vortex, missing only the region with the very highest values of PV. The proxy O_3 field, calculated from the PV field in Plate 4b and the quadratic coefficients defining the fit in Plate 4a, is plotted in Plate 4c. As expected from the monotonic PV/O_3 relation in Plate 4a, the O_3 field is essentially the reverse of the PV field – with low O_3 inside the vortex, and high O_3 outside the vortex.

Extending this illustration to other days, Plate 5 shows the POAM III O_3 mixing ratios at 500 K and quadratic PV/O_3 fits for four different days during the SOLVE campaign. This figure illustrates the gradually changing PV/O_3 relation over the course of the winter. Although similar information about the data can be derived from Plate 3, we focus here on the quadratic fits to the data. The most salient point about this figure is that for all of these days, a quadratic fit appears to match the data quite well, on average. On 20 December, edge and in-V mixing ratios are higher than out-V, due to enhanced diabatic descent inside the vortex. The fit shows a slight enhancement of edge mixing ratios over in-V mixing ratios, but this is somewhat uncertain since, as shown in Plate 1, only a small fraction of the POAM measurements at this time occurred inside the inner edge of the vortex. Thus, extrapolation of this quadratic to substantially higher values of PV is expected to be less certain than, for instance, extrapolation to lower values of PV. By the end of January, the enhancement of edge O_3 mixing ratios over those both outside and inside the vortex is clear, the result of enhanced diabatic descent on the edge bringing down O_3-rich air. By late February, the fits indicate mixing ratios inside the vortex that are significantly less than outside, a result expected only in the presence of chemical O_3 loss. On 20 March, even though POAM sampled a wide range of PV, fewer points define the quadratic inside the vortex, suggesting higher uncertainty for the fit at this time.

Applying the fits shown in Plate 5 to the UKMO PV fields, we generated the proxy O_3 maps shown in Plate 6. Overall, these maps are consistent with the interpretation of the plots at the POAM latitudes discussed above. That is, areas of highest O_3 in December through February form a collar near the vortex edge, where descent of O_3-rich air dominates. The areas of lowest O_3 in February lie inside the vortex, and signify chemical O_3 loss during the winter. On March 20, the vortex was elongated and split into two areas of high PV (and relatively low O_3), resulting in the double-lobed appearance to this map. These maps also illustrate, however, the potential for error when using the mapping technique to infer O_3 at latitudes far from the original measurements. Consider, for instance, the map for 20 January 2000. The apparent intrusion of air with high O_3 mixing ratios from the vortex edge to the pole near Greenland is an artifact due to anomalous structure in the UKMO PV field for this day. Indeed, the proxy O_3 mixing ratio at 500 K on 20 January, interpolated to the location of Eureka (79.9°N, -85°E), was higher by about 15% than the sonde measurement for that day.

At the other extreme, the very low (~2.2 ppmv) proxy O_3 mixing ratios on 20 January near 80°N latitude are also an artifact, and are lower than actual measurements, for instance at Ny Ålesund (see section 4). These low mixing ratios result from an extrapolation of the PV/O_3 relation to higher PV values and latitudes than were observed. The primary reason for this is that because of the dynamically induced higher O_3 on the edge of the vortex, the mapping technique causes O_3 to monotonically decrease at higher values of PV that are not sampled by POAM, rather than

to level off to some extent inside the vortex. Using higher order polynomials for the PV/O_3 fits can alleviate this type of problem somewhat, but introduces other artifacts into the analysis. This effect is exacerbated by the fact that the return of sunlight to the POAM measurement latitude (~64°N) in January caused some chemical loss at 500 K (see Plate 3; also [*Hoppel et al*., this issue]) inside the vortex. Even though such loss could not yet have occurred at the higher latitudes still in darkness, the mapping technique generalizes it to the entire vortex, and in fact extrapolates to even lower O_3 values at the higher PV values. In the next section, we explore in detail the effects of such errors on the validity of the reconstructed fields.

4. Validation of the Method

To validate the PV mapping technique with POAM data, we have extensively compared the proxy O_3 profiles generated using the method above to profiles obtained from balloon-based electrochemical concentration cell and Brewer-Mast ozonesondes and the Halogen Occultation Experiment (HALOE). Comparisons were made by interpolating the proxy O_3 horizontally and vertically to the correlative measurement locations. These comparisons included locations both well north and well south of the actual POAM III measurement locations, and both outside and inside the polar vortex. Ozonesonde profiles were obtained from a sonde network operating within the framework of the THESEO 2000-EuroSOLVE project. For this work, we used data from 29 stations in Europe, North America, and Russia. Station locations and the number of profiles used from each are listed in Table 1. All data incorporated in our analysis have been quality controlled in real time during the SOLVE campaign, by daily visual inspection of profiles. The time series data from Ny Ålesund (see below) have also passed a more rigorous, post-mission quality control process. HALOE version 19 O_3 data were obtained from the HALOE home page (http://haloedata.larc.nasa.gov/). The O_3 profiles were placed on potential temperature grids using the temperatures and pressures provided with the sonde (measured by radiosonde) and HALOE (NCEP) data sets.

Plate 7 shows representative comparisons between individual ozonesonde profiles at three different locations and the proxy O_3 profiles (determined by interpolation of the proxy O_3 field on the UKMO grid to the sonde location). For this example, we have chosen to show results from stations that were roughly 14° north (Ny Ålesund), 17° south (Hohenpeissenberg), and 37° south (Izana) of the POAM measurements. In general the agreement with the sondes is excellent, with the proxy even capturing the steep lower stratospheric gradient in the O_3 profile at Izana (28.4°N). The discrepancy above 700 K in the Izana comparisons is primarily due to the fact that at this low latitude and these high altitudes, O_3 is no longer a passive tracer.

To quantify the sonde results, we have carried out a statistical analysis, calculating the average differences between the proxy and the sonde profiles for each of the measurements listed in Table 1. Plate 8 shows the average difference profile for these comparisons, as well as the individual differences and standard deviation of the mean (which is equivalent to the uncertainty in the mean). These results show that for the early to mid-winter data included here, the proxy O_3 profiles on average agree with the sondes to better than 5% below about 800 K. This agreement is particularly noteworthy given the large range of sonde locations compared to the relatively localized POAM measurement latitudes. Approximately 4.4% of the comparisons shown in Plate 8 include proxy O_3 data that were derived from an extrapolation of the PV/O_3 quadratic fit beyond the range of PV values actually sampled by POAM (75 points out of 1720).

The comparisons including these extrapolated points are fairly evenly distributed among the entire set of comparisons, and do not significantly affect the overall averages.

To better understand the latitude dependence of the quality of the proxy profiles, we have compared the proxy O_3 to more than nine hundred O_3 profiles measured by HALOE, at the latitudes and times shown in Figure 2. The latitude dependence of the differences between HALOE and the proxy O_3 is shown in Plate 9 for four different potential temperature levels. These comparisons show that between 500 K and 850 K, the proxy O_3 generally agrees with the HALOE data remarkably well at latitudes poleward of 30°N (see below), but more poorly at equatorial latitudes. The larger differences at the lower latitudes probably have two causes. First, increasing uncertainty in the UKMO PV field at these latitudes is likely to contribute to errors in the PV/O_3 analysis. Second, these latitudes correspond to PV values well outside the range sampled by POAM, where the quadratic relation may no longer hold (note that comparisons where the proxy O_3 was determined from an extrapolation of the PV/O_3 quadratic fit beyond the PV range sampled by POAM are denoted in black). At 650 K and above, the results at the lower latitudes may also be affected by the fact that increasing sunlight will cause O_3 to transition away from a dynamically controlled situation [*Garcia and Solomon*, 1985], increasing the error in the PV/O_3 analysis. Although agreement is worse at 1250 K than at the lower altitudes, it is still quite reasonable poleward of 30°N.

To quantify these comparisons, Figure 3 shows the statistical results for all events (724) poleward of 30°N. Comparisons including proxy O_3 derived from an extrapolation of the PV/O_3 quadratic fit beyond the PV range sampled by POAM constitute about 20% of the data points at latitudes poleward of 30°N; their removal does not significantly alter the conclusions stated here. Like the sonde comparisons, agreement is impressive, with differences often less than 5% below 1100 K. The differences increase at the highest altitudes, most likely because of the lack of dynamical control at these altitudes as sunlight returns to the polar region. The large differences at 400 K in part reflect real differences between the POAM and HALOE data which have not yet been resolved (Rusch *et al.*, Validation of POAM III O_3: Comparison to ozonesonde and satellite data, submitted to *J. Geophys. Res.*, 2001). However, near 400 K the documented differences between POAM and HALOE are only at the 10% level, and cannot entirely explain either the average differences seen in Figure 3, or the marked increase in the variability of the comparisons at 400 K. We believe the deterioration in the comparisons at 400 K may result from increased mixing of air parcels at and below this altitude, where the effective diffusivity is generally higher than at higher altitudes [Haynes and Shuckburgh, 2000]. Variable small-scale mixing could change the PV/O_3 relationship as a function of geographic location, so that the fit derived from the POAM data would not necessarily apply to the location of the HALOE (or sonde) measurements. This would suggest that for the SOLVE winter, the lower altitude limit for the PV mapping technique employed here is around 400-450 K. Confirming this speculation requires more investigation, and is beyond the scope of this paper.

To probe more deeply into the quality of the PV/O_3 reconstruction at latitudes poleward of the POAM measurements, and to evaluate the proxy O_3 in regions of chemical O_3 loss, we have compared in detail the proxy O_3 to ozonesonde measurements made at Ny Ålesund. At 78.9°N and 12°E, this station is often located under the center of the NH vortex, where one might expect O_3 loss to maximize. Indeed, as noted earlier, O_3 loss of more than 70% during the SOLVE

winter has been inferred above Ny Ålesund [*Sinnhuber et al.*, 2000]. Figure 4 shows the evolution of O_3 mixing ratios measured by sonde above Ny Ålesund at four different potential temperature levels between 450 and 750 K, from late November through April. Superimposed are the proxy O_3 values, interpolated to the latitude and longitude of Ny Ålesund. Throughout most of the winter, at all of these potential temperature levels, the agreement is remarkable, with mean differences ranging from about +5% to –7%. These results indicate that even at latitudes significantly poleward of the POAM measurements, and well inside the vortex, the PV mapping yields reasonable O_3 values. In particular, the proxy field captures the variations in O_3 at 450 K until early March and at 500 K until late March, including the decline caused by chemical loss processes. There are two noteworthy regions of disagreement. At 450 K and 500 K, proxy O_3 values at the end of January and beginning of February are generally somewhat lower than the sonde data. As discussed above with regard to Plate 6, this results from errors in the in-V reconstruction stemming largely from the fact that the air parcels sampled by POAM have been exposed to more sunlight, and thus more chemical processing leading to O_3 loss, than air over Ny Ålesund, even if they are at similar equivalent latitudes. In two cases, this is compounded by an extrapolation of the PV/O_3 curve beyond the range of PV sampled by POAM. This comparison thus emphasizes the need for caution when interpreting the proxy O_3 results in regions where geographic gradients due to photochemistry are significant, particularly if the proxy is derived from extrapolations beyond the sampled range of PV. The other notable disagreement occurs at 450 K near day 90, where proxy O_3 is significantly higher than sonde O_3. At this time, POAM was sampling primarily on the edge of the vortex, and the mapping thus failed to capture the morphology of the substantial O_3 loss that occurred at higher equivalent latitudes. Furthermore, the vortex was evolving rapidly at this time, increasing the uncertainty in the PV mapping analysis. Note, however, that the increase in O_3 near day 80 (20 March), as the vortex shifted away from Ny Ålesund, was captured fairly well by the PV/O_3 analysis.

The comparisons presented here show that overall, the proxy O_3 profiles are in excellent agreement with correlative observations, and can be used extensively for scientific investigations. Caution is required, however, when there are significant errors in our knowledge of the PV/θ fields, or in our knowledge of the PV/O_3 relation. The latter error, which is the most prevalent, can arise for a number of different reasons. First, this will often result when the range of PV sampled by the instrument is too narrow to adequately extrapolate outside this range. Second, the PV/O_3 relation may not follow closely enough the quadratic curve that we use to define it, instead being better defined by another analytic form. Third, if the PV/θ field is changing rapidly (e.g., through diabatic processes), the PV/O_3 relation defined by a seven-day period will average over these PV variations. Fourth, it may simply be inappropriate to assume a single (quadratic or otherwise) PV/O_3 relation. This will be the case, for instance, when O_3 is in photochemical control, and is thus not expected to strictly correlate with PV. For example, we expect the analysis to work less well in the middle to upper stratosphere in summer, and also in the presence of the anticyclonic low O_3 pockets that occur in the winter middle stratosphere [*Manney et al*., 1995b; *Nair et al.,* 1998; *Morris et al*., 1998]. For the latter situation, there may be a perfectly valid quadratic that describes the PV/O_3 relation everywhere except near the low O_3 pockets, where the proxy O_3 would overestimate the observed O_3. Note, however, that even in the presence of chemical changes, such as polar O_3 loss, the mapping technique will produce valid results as long as O_3 and PV are well-correlated within the time period of the analysis, and

as long as the observations fulfill the other requirements such as adequate sampling of the PV/θ field (e.g., Figure 4).

5. Application of the Method

The results above confirm the validity of the PV mapping technique for deriving proxy O_3 values from the POAM III data at most times and locations during the NH winter poleward of 30°N. These results can be used for a variety of purposes, and are particularly relevant in times (such as the SOLVE winter) when high vertical resolution, global, O_3 measurements are lacking. In general, using the proxy O_3 will improve analyses that rely on climatological profiles for lack of actual data. For instance, the proxy O_3 data have been used to initialize calculations for investigations of O_3 photochemical loss during the winter [*Hoppel et al.*, this issue], and can be used to improve satellite data retrievals which require a priori O_3 profiles, such as those from the TOMS instrument. When combined with data from other instruments such as HALOE or SAGE, the analysis can be improved at the lower latitudes. We are currently using this strategy as one means of generating global stratospheric O_3 fields for inclusion in the Navy's operational weather prediction system (NOGAPS [*Hogan and Rosmund*, 1991]). In this section, we describe the application of POAM PV mapping results to calculations of photolysis rates relevant to SOLVE investigations.

One of the primary goals of the SOLVE campaign was to investigate O_3 loss processes using the numerous measurements of stratospheric species along the DC-8 and ER-2 flight paths. To put those measurements into the context of a detailed photochemistry scheme requires knowledge of the rate coefficients for the relevant photolytic reactions; i.e., the j-values. The j-values can be calculated most directly if one measures the solar actinic flux that is transmitted through the atmosphere to the aircraft location from all directions, at the appropriate wavelengths. This is accomplished by the Scanning Actinic Flux Spectroradiometer (SAFS) instruments [*Shetter and Müller*, 1999] on the DC-8 for fifteen molecules of interest. A more indirect determination of the j-values is to measure the O_3 column above the aircraft, and to use this information to deduce the transmission through the atmosphere of the radiation responsible for the photolysis. The principal sources of overhead O_3 information during previous ER-2 campaigns have been the in-situ Composition and Photodissociative Flux Measurement (CPFM) [*McElroy*, 1995], and the TOMS satellite measurements (from which a climatological tropospheric column must be subtracted) [*McPeters et al*., 1998]. A drawback to using these measurements, however, is that they become much less reliable or unavailable at high solar zenith angles (SZAs). Thus, accurately determining O_3 columns over the ER-2 at high SZAs was one of the primary motivating factors for applying the PV mapping technique to the POAM III data.

The POAM III reconstructed O_3 fields have been used to create consistent j-value data sets for the entire campaign, independent of limitations at high SZAs. This has been done independently by two different groups, at the Applied Physics Laboratory (APL) and at the Jet Propulsion Laboratory (JPL). In order to calculate accurate j-values, it is necessary that the reconstructed O_3 at and above the aircraft flight track be accurate. The validation discussion above showed that statistically, the reconstructed profiles interpolated to ozonesonde and HALOE measurement locations compared very well to the observations. We investigated the reliability of the PV mapping results for determining O_3 at the aircraft location by comparing the proxy O_3 to in situ O_3 measurements from the ozone photometer onboard the ER-2 [*Proffit and McLaughlin*, 1983;

Richard *et al*., 2001]. For these comparisons, some representative examples of which are shown in Plate 10, the proxy O_3 was interpolated horizontally and vertically to the ER-2 flight tracks. Plate 10 reveals excellent agreement between the proxy O_3 and ER-2 observations, even during the rapid altitude changes (dips) of the aircraft, as expected from the comparisons shown above.

To illustrate the reliability of the j-value calculations themselves, Figure 5 compares the APL calculations [*Swartz et al*., 1999] appropriate for the DC-8 flight on 3 March 2000 to the j-values derived using actinic flux measurements from the SAFS measurement, for the $O_3 \rightarrow O(^1D)$ reaction. The j-values derived from the POAM reconstruction analysis match those derived from the SAFS measurements quite well, generally agreeing to within 10% or better. Also shown are the j-values determined using TOMS measurements of total ozone. These also match the SAFS determinations well, although not quite as well as the POAM-based calculations for this particular flight. It should be noted that for the TOMS calculations, climatological O_3 profiles were scaled to the TOMS total column, so that the O_3 column below the DC-8 could be subtracted off. Likewise, climatological profiles were used to extend the POAM measurements down to the DC-8 flight altitude. When averaged over the entire campaign, the APL(TOMS) calculations of $j(O_3)$ at SZA>85° exceeded determinations based on the SAFS data by ~13±3%. The APL(POAM) calculations on average agreed better with the SAFS determinations, exceeding them by only 3±2%. With regard to these results, however, it is important to note that the TOMS total O_3 retrieval has not been optimized for the high latitudes and SZAs encountered during the SOLVE campaign. At lower SZAs, APL(TOMS) and APL(POAM) provided more comparable levels of agreement with SAFS.

Plate 11 demonstrates the utility of the j-value calculations based on the POAM reconstruction for ER-2 flights. In this figure we compare JPL j-value calculations for the photolysis of Cl_2O_2 based on column O_3 determined from the POAM reconstruction and the CPFM measurements. We show two different derivations for the POAM reconstruction, including calculations based solely on the POAM proxy data, as well as calculations based on the proxy data scaled to the TOMS total column O_3. For the latter case, the reconstructed O_3 profiles are scaled such that the total column abundance of the proxy profile, which is extended below the POAM measurements with a climatological profile, matches the TOMS total column. For this case, the proxy, scaled proxy and CPFM j-value determinations match quite well throughout most of the flight. However, at the highest SZAs, between about 11.5 and 14 GMT, the CPFM values are unavailable. Thus, the proxy determination serves to fill in this time gap. Similar results are seen for other flights and other j-values: in general, there is good agreement between estimates of overhead ozone, and thus j-values, based on the POAM reconstruction and the CPFM data, for SZA less than about 85°. For the largest SZA, however, the reconstruction with POAM data provides a more accurate method of determining j-values than simply relying on climatological data, as has been the practice in the past.

6. Summary

For each day during the 1999-2000 winter, we have used the relation between PV and O_3 mixing ratio to calculate semi-global (NH only) three-dimensional O_3 fields. The work presented here represents the first demonstration of the PV mapping technique applied to solar occultation measurements at high equivalent latitudes over the course of an entire winter. We have extensively compared the proxy O_3 so generated to profiles obtained from ozonesondes and

HALOE. Comparisons were made by interpolating the proxy O_3 horizontally and vertically to the correlative measurement locations. These comparisons included locations both well north and well south of the actual POAM III measurement locations, and both outside and inside the polar vortex. On average, the proxy O_3 agrees with the correlative observations to better than ~5%, at potential temperatures below about 900 K, and at latitudes above about 30°N (i.e., in the region where O_3 is dynamically controlled). These results demonstrate the reliability of the reconstructed global fields using the PV mapping technique. The POAM III proxy ozone fields have been used to estimate O_3 profiles for the computation of photolysis rates along the SOLVE aircraft flight tracks.

Finally, Plate 12 shows the proxy fields at 500 K throughout the SOLVE winter in 5-day increments. This figure graphically illustrates the changing ozone field as dynamical and chemical processes perturb the polar region over the course of the winter. Air descending in and on the edge of the vortex causes O_3 mixing ratios to increase at 500 K, and is responsible for the ring at the edge of the vortex that is so prominent in most of the panels. Persistent chemical O_3 loss inside the vortex begins in late January at POAM latitudes, and continues through March, as indicated by the transition toward the blue end of the color scale. Toward the end of March the vortex begins to break down at 500 K, and the two pockets of low ozone on 21 March coincide with the two branches of the vortex at this time. Even as late as 20 April, there are persistently low O_3 mixing ratios coinciding with the highest PV values, presumably remnants of the low-O_3 regions which formed during the winter inside the vortex. As noted above, detailed interpretation of the proxy fields requires caution when mechanisms responsible for ozone variability depend on factors other than equivalent latitude. In spite of this caveat, and other potential errors discussed above, the proxy fields illustrate the versatility and applicability of the solar occultation observations for O_3 loss investigations. Furthermore, by presenting a 3D picture of the changing Arctic O_3, they provide information easily accessible to the general public. The proxy fields present a qualitative picture of semi-global, vertically resolved O_3 variations throughout the winter in the lower stratosphere, a picture that is not directly available from any of the currently operational satellite instruments. This method is easily extended to other winters measured by POAM II and POAM III, and will be applicable to measurements from SAGE III once it is launched. Ideally, POAM III data will be combined with HALOE or SAGE II to improve results at the lower latitudes, and with future SAGE III measurements to improve PV-sampling at the highest latitudes.

Acknowledgements
This work was supported by NASA grant N00014-97-1-G018 and by the NASA Scientific Data Purchase program through contract # NAS13-99031. We thank G. Manney for helpful discussions, R. Shetter for providing the SAFS data, and M. Rex for providing easy access to ozonesonde data during the SOLVE campaign. Version 3.0 POAM III data can be obtained from the NASA Langley Research Center EOSDIS Distributed Active Archive Center. We would like to acknowledge the following providers of ozonesonde data: V. Dorokhov (Central Aerological Observatory, Russia), M. Gil (Icelandic Meteorological Office and Instituto Nacional de Tecnica Aeroespacial), I. S. Mikkelsen (Danish Meteorological Institute; Jaegersborg, Scoresbysund, Thule), Z. Litynska (IMWM, Legionowo), R. Stubi (Meteoswiss/Payerne), T. Turunen (Finnish Meteorological Institute, Sodankyla), and G. Vaughan (University of Wales, Aberystwyth).

References

Allaart, M.A.F., H. Kelder, and L.C. Heijboer, On the relation between ozone and potential vorticity, *Geophys. Res. Lett.* 20, 811-814, 1993.

Bevilacqua, R.M., *et al.*, POAM III PSC observations during the 1999/2000 northern hemisphere winter, *J. Geophys. Res.*, 2001 (this issue).

Butchart, N. and E.E. Remsberg, The area of the stratospheric polar vortex as a diagnostic for tracer transport on an isentropic surface, *J. Atmos. Sci.* 43, 1319-1339, 1986.

Garcia, R.R., and S. Solomon, The effect of breaking gravity waves on the dynamics and chemical composition of the mesosphere and lower thermosphere, *J. Geophys. Res.* 90, 3850-3868, 1985.

Haynes, P. and E. Shuckburgh, Effective diffusivity as a diagnostic of atmospheric transport, 1. Stratosphere, *J. Geophys. Res.* 105, 22,777-22,794, 2000.

Hogan, T. and T. Rosmund, The description of the Navy Operational Global Atmospheric Prediction Systems spectral forecast model, *Mon. Weather Rev*. 119, 1786-1815, 1991.

Hoppel, K.W., *et al*., POAM III observations of Arctic ozone loss for the 1999/2000 winter, *J. Geophys. Res.*, 2001 (this issue).

Lait, L.R., An alternative form for potential vorticity, *J. Atmos. Sci.* 51, 1754-1759, 1994.

Lait, L.R., *et al*., Reconstruction of O_3 and N_2O fields from ER-2, DC-8, and balloon observations, *Geophys. Res. Lett.* 17, 521-524, 1990.

Leovy, C.B., C-R. Sun, M.H. Hitchman, E.E. Remsberg, J.M. Russell, III, L.L. Gordley, J.C. Gille, and L.V. Lyjak, Transport of ozone in the middle stratosphere: Evidence for planetary wave breaking, *J. Atmos. Sci.* 42, 230-244, 1985.

Lucke, R.L., *et al*., The Polar Ozone and Aerosol Measurement (POAM) III instrument and early validation results, *J. Geophys. Res.* 104, 18757-18799, 1999.

Lumpe, J.D., *et al*., Comparison of POAM III ozone measurements with correlative aircraft and balloon data during SOLVE, *J. Geophys. Res.*, 2001 (this issue).

Manney, G.L., *et al*., Comparison of satellite ozone observations in coincident air masses in early November 1994, *J. Geophys. Res.* 106, 9923-9943, 2001.

Manney, G.L., and J.L. Sabutis, Development of the polar vortex in the 1999-2000 Arctic winter stratosphere, *Geophys. Res. Lett.* 27, 2589-2592, 2000.

Manney, G.L., H.A. Michelsen, M.L. Santee, M.R. Gunson, F.W. Irion, A.E. Roche, and N.J. Livesey, Polar vortex dynamics during spring and fall diagnosed using trace gas observations

from the Atmospheric Trace Molecule Spectroscopy instrument, *J. Geophys. Res.* 104, 18,841-18,866, 1999.

Manney, G.L., J.C. Bird, D.P. Donovan, T.J. Duck, J.A. Whiteway, S.R. Pal, and A.I. Carswell, Modeling ozone laminae in ground-based Arctic wintertime observations using trajectory calculations and satellite data, *J. Geophys. Res.* 103, 5797-5814, 1998.

Manney, G.L., L. Froidevaux, J.W. Waters and R.W. Zurek, Evolution of microwave limb sounder ozone and the polar vortex during winter, *J. Geophys. Res.* 100, 2953-2972, 1995a.

Manney, G.L., *et al*., Formation of low ozone pockets in the middle stratosphere anticyclone during winter, *J. Geophys. Res.* 100, 13,939-13,950, 1995b.

McElroy, C. T., A spectroradiometer for the measurement of direct and scattered solar irradiance from on-board the NASA ER-2 high-altitude research aircraft, *Geophys. Res. Lett*., 22, 1361-1364, 1995.

McPeters, R., *et al*., Earth Probe Total Ozone Mapping Spectrometer (TOMS) data products user's guide, NASA/TP-1998-206895, NASA, Goddard Space Flight Center, Greenbelt, Maryland, 1998.

Morris, G.A., S.R. Kawa, A.R. Douglass, M.R. Schoeberl, L. Froidevaux, and J. Waters, Low-ozone pockets explained, *J. Geophys. Res.* 103, 3599-3610, 1998.

Nair, H., M. Allen, L. Froidevaux, and R.W. Zurek, Localized rapid ozone loss in the northern winter stratosphere: An analysis of UARS observations, *J. Geophys. Res.* 103, 1555-1571, 1998.

Nash, E.R., P.A. Newman, J.E. Rosenfield, and M.R. Schoeberl, An objective determination of the polar vortex using Ertel's potential vorticity, *J. Geophys. Res.* 101, 9471-9478, 1996.

Proffitt, M. H., and R. J. McLaughlin, Fast-response dual-beam UV absorption ozone photometer suitable for use on stratospheric balloons, *Rev. Sci. Instrum*., 54, 1719-1728, 1983.

Randall, C.E., *et al*., Preliminary results from POAM II: Stratospheric ozone at high northern latitudes, *Geophys. Res. Lett.* 22, 2733-2736, 1995.

Redaelli, G., *et al*., UARS MLS O_3 soundings compared with lidar measurements using the conservative coordinates reconstruction technique, *Geophys. Res. Lett.* 21, 1535-1538, 1994.

Richard, E.C., *et al*., Severe chemical ozone loss inside the Arctic polar vortex during winter 1999-2000 inferred from in-situ airborne measurements, *Geophys. Res. Lett.*, 28, 2197-2200, 2001.

Santee, M.L., G.L. Manney, N.J. Livesey, and J.W. Waters, UARS Microwave Limb Sounder observations of denitrification and ozone loss in the 2000 Arctic winter, *Geophys. Res. Lett.* 27, 3213-3216, 2000.

Schoeberl, M.R., *et al*., Reconstruction of the constituent distribution and trends in the Antarctic polar vortex from ER-2 flight observations, *J. Geophys. Res.* 94, 16,815-16,845, 1989.

Shetter, R. E., and M. Müller, Photolysis frequency measurements using actinic flux spectroradiometry during the PEM-Tropics mission: Instrumentation description and some results, *J. Geophys. Res.*, 104, 5647-5661, 1999.

Sinnhuber, B.-M., *et al*., Large loss of total ozone during the Arctic winter of 1999/2000, *Geophys. Res. Lett.* 27, 3473-3476, 2000.

Swartz, W. H., S. A. Lloyd, T. L. Kusterer, D. E. Anderson, C. T. McElroy, and C. Midwinter, A sensitivity study of photolysis rate coefficients during POLARIS, *J. Geophys. Res*., 104, 26,725-26,735, 1999.

Swinbank, R., and A. O'Neill, A stratosphere-troposphere data assimilation system, *Mon. Weather Rev.*, 122, 686-702, 1994.

Figures

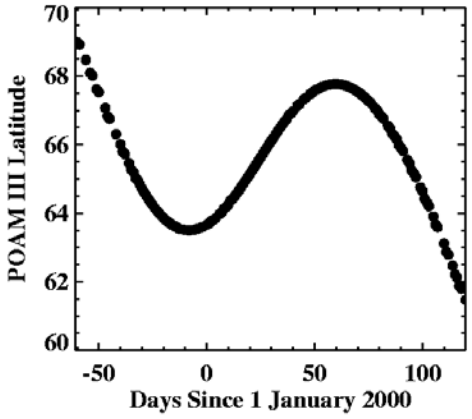

Figure 1. Latitudes of the NH POAM measurements from 1 November 1999 through 30 April 2000.

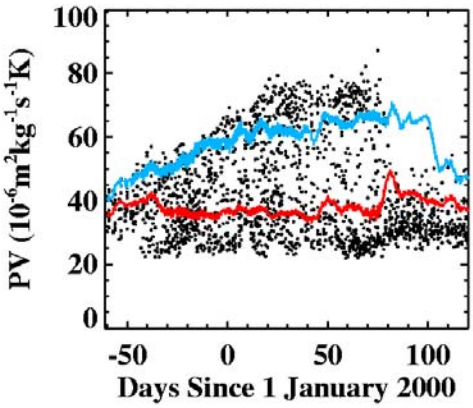

Plate 1. Potential vorticity of the NH POAM measurements from 1 November 1999 through 30 April 2000. The inner and outer boundaries of the vortex edge region are denoted in blue and red, respectively.

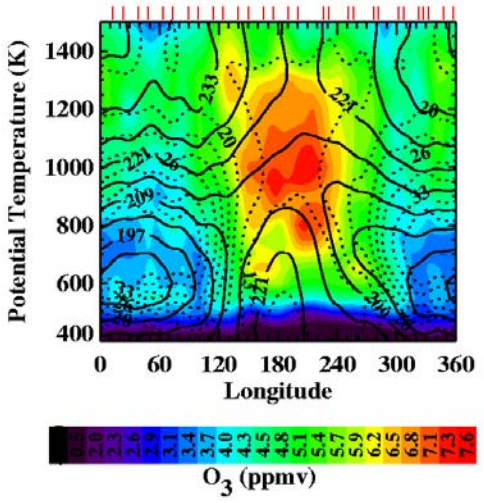

Plate 2. Representative contour map made from POAM III O_3 measurements from 24-26 December 1999, at a latitude of 63.5°. The temperature (K) and modified PV (10^{-6} K m^2 kg^{-1} s^{-1}) [*Lait*, 1994] derived from UKMO data are superimposed as solid and dotted lines, respectively. POAM profile locations are given by the red marks above the top horizontal axis.

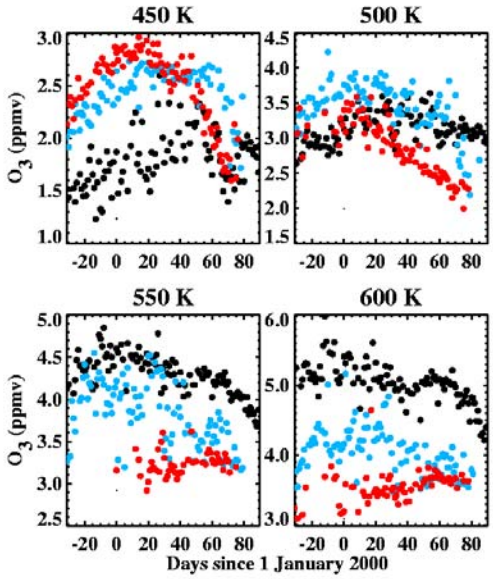

Plate 3. Daily average POAM III O_3 mixing ratios inside the vortex (red), on the edge of the vortex (blue) and outside the vortex (black) from 1 December 1999 through 31 March 2000, at the potential temperatures noted in each panel.

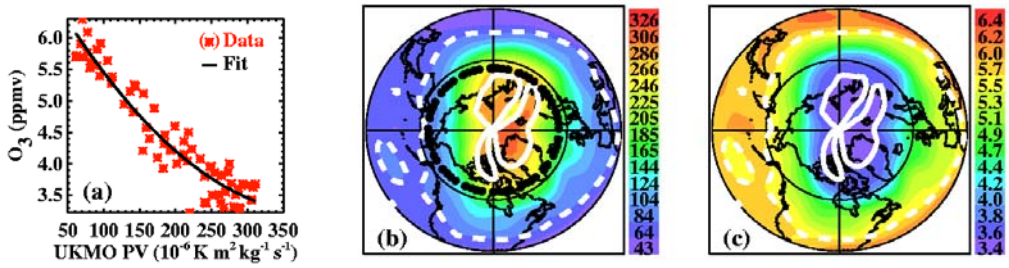

Plate 4. (a) POAM III O_3 mixing ratios at 650 K from 29 December through 4 January 2000 (red asterisks), plotted against the UKMO PV interpolated in time and space to the POAM measurement locations. Superimposed is a quadratic fit to the data. (b) UKMO PV field on 1 January 2000 on the 650 K potential temperature surface. Latitude lines are drawn at 30°N and 60°N, and East longitudes increase counterclockwise from 0° on the right. POAM measurement locations from 29 December 1999 to 4 January 2000 are denoted by the black dots. Solid (dashed) white contours denote the geographic boundaries inside (outside) of which the PV values were higher (lower) than those sampled by POAM. (c) The proxy O_3 field for 1 January 2000, calculated as described in the text. The color scales refer to PV (10^{-6} m^2 kg^{-1} s^{-1} K) in (b) and to O_3 mixing ratio (ppmv) in (c).

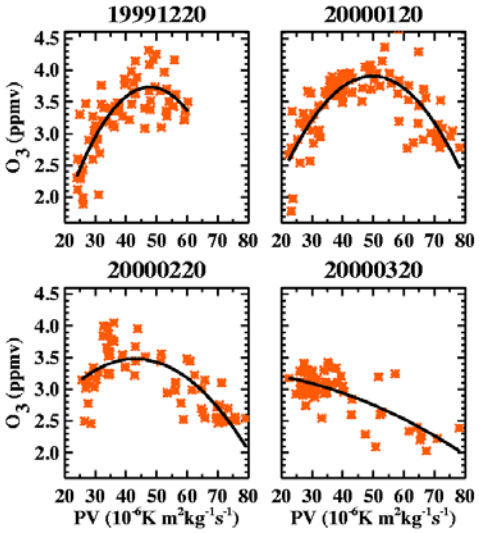

Plate 5. As in Plate 4a, but for the 500 K potential temperature level, for the days noted in each panel.

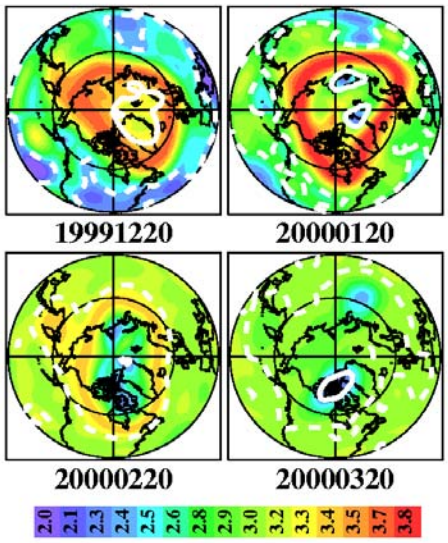

Plate 6. As in Plate 4c, but corresponding to the plots in Plate 5.

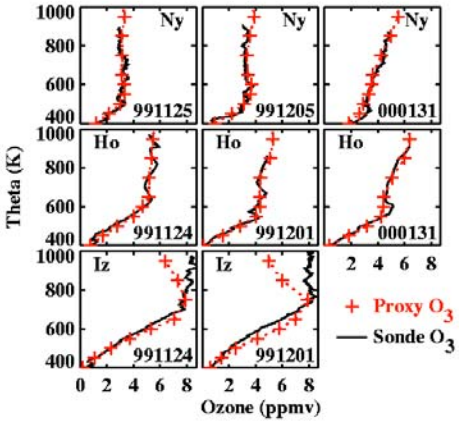

Plate 7. Representative examples of individual profile comparisons between the proxy O_3 interpolated to the sonde location (red, +) and the sonde profile (black) at Ny Ålesund (Ny), Hohenpeissenberg (Ho), and Izana (Iz), on the dates (yymmdd) shown in each panel.

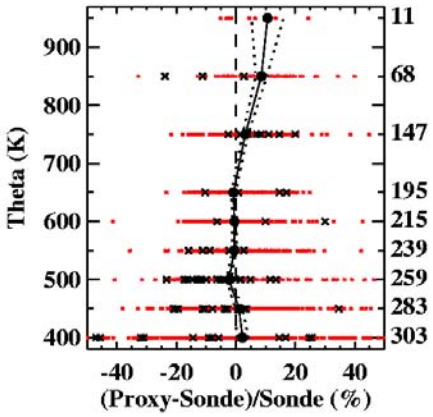

Plate 8. Statistical results for all ozonesonde comparisons between 22 November 1999 and 1 February 2000 shown as the average difference profile (solid line with dots) and the standard deviation of the mean (dotted lines), with the individual differences overplotted as red points (black x marks denote individual differences where the proxy O_3 was derived from an extrapolation of the PV/O_3 quadratic fit beyond the range of PV values actually sampled by POAM). The number of comparisons included at each potential temperature level is given on the right vertical axis.

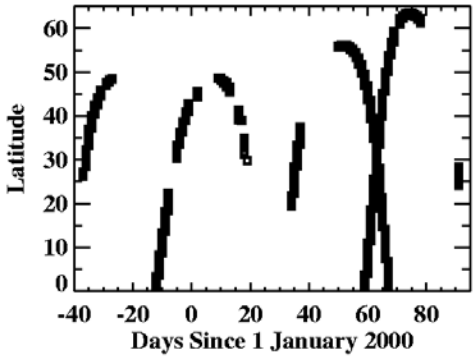

Figure 2. HALOE measurement latitudes in the NH during SOLVE, from late November, 1999 through March, 2000.

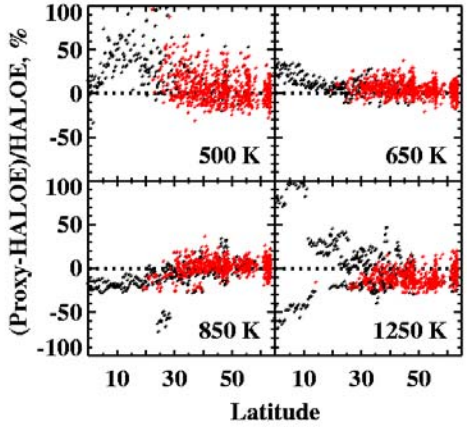

Plate 9. Latitude dependence of the differences between HALOE and the proxy O_3 for events noted in Figure 2, at the potential temperature levels denoted in each panel. Comparisons including proxy O_3 derived from extrapolation of the PV/O_3 fit beyond the range of PV sampled by POAM are indicated in black; all other comparisons are indicated in red.

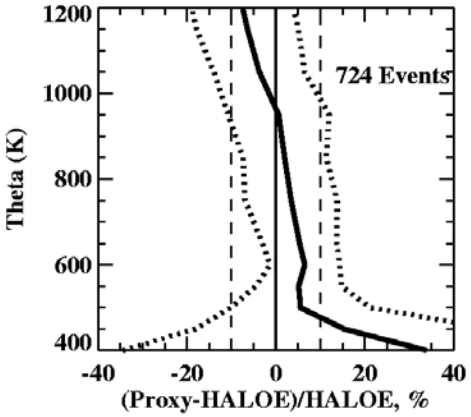

Figure 3. Statistical differences (heavy solid line) for events north of 30°N in the proxy-HALOE comparisons. Dotted lines are the standard deviation of the distribution. The standard deviations of the mean are approximately the thickness of the heavy solid line. Dashed lines are plotted at ±10% for guidance.

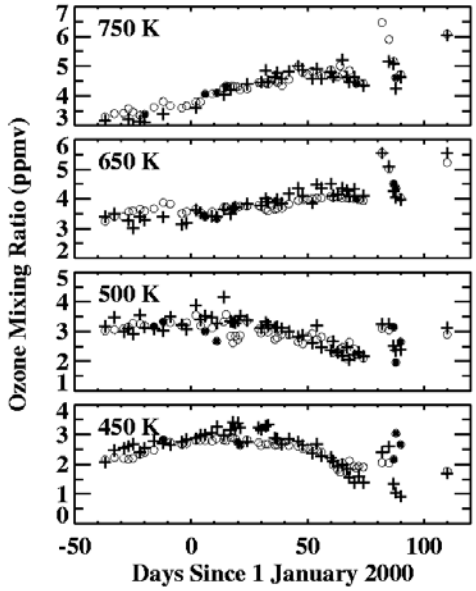

Figure 4. Evolution of O_3 mixing ratios measured by ozonesonde over Ny Ålesund (plus symbols), at the different potential temperature levels noted in each panel, compared to the proxy O_3 derived for the location of this station (open circles). Proxy O_3 data derived from extrapolation of the PV/O_3 quadratic fit beyond the range of PV sampled by POAM are denoted by the filled circles.

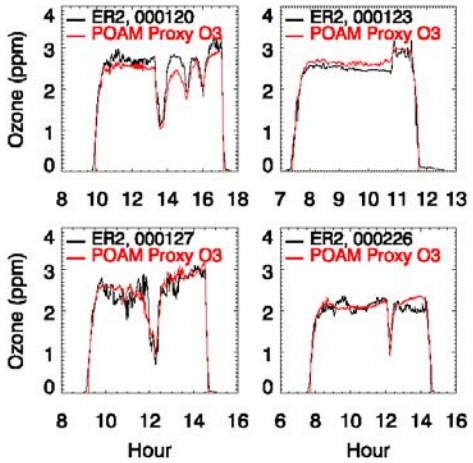

Plate 10. Comparison of the reconstructed O_3 interpolated to the ER-2 flight location (red) and the in-situ measurements from the ozone photometer onboard the ER-2 (black) during the flight on the date (yymmdd) noted in each panel. The sharp dips in the O_3 measurements correspond to rapid altitude changes by the ER-2.

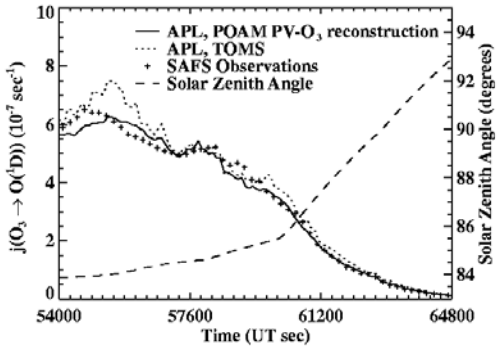

Figure 5. Comparison of O_3 photolysis j-values determined by the APL group based on the POAM reconstructed O_3 (solid) and the TOMS total column measurements (dotted) to calculations based on SAFS actinic flux observations (+) for the DC-8 flight on 3 March 2000. The SZA variation along the flight track is denoted by the dashed line.

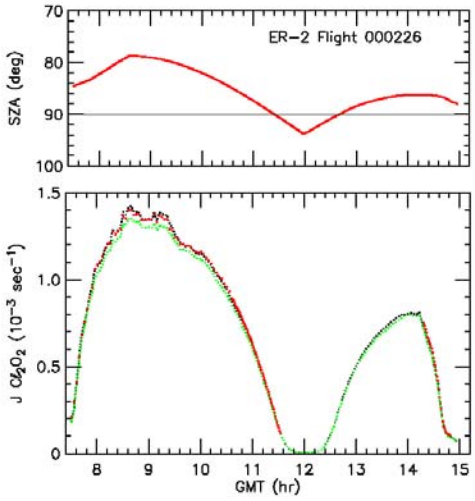

Plate 11. Comparison of Cl_2O_2 photolysis j-values determined by the JPL group based on the POAM reconstructed O_3 (green) and the POAM reconstructed O_3 scaled to the TOMS measurements (black), to calculations based on the CPFM data (red) for the ER-2 flight on 26 February 2000. The SZAs of the measurements are noted in the top panel.

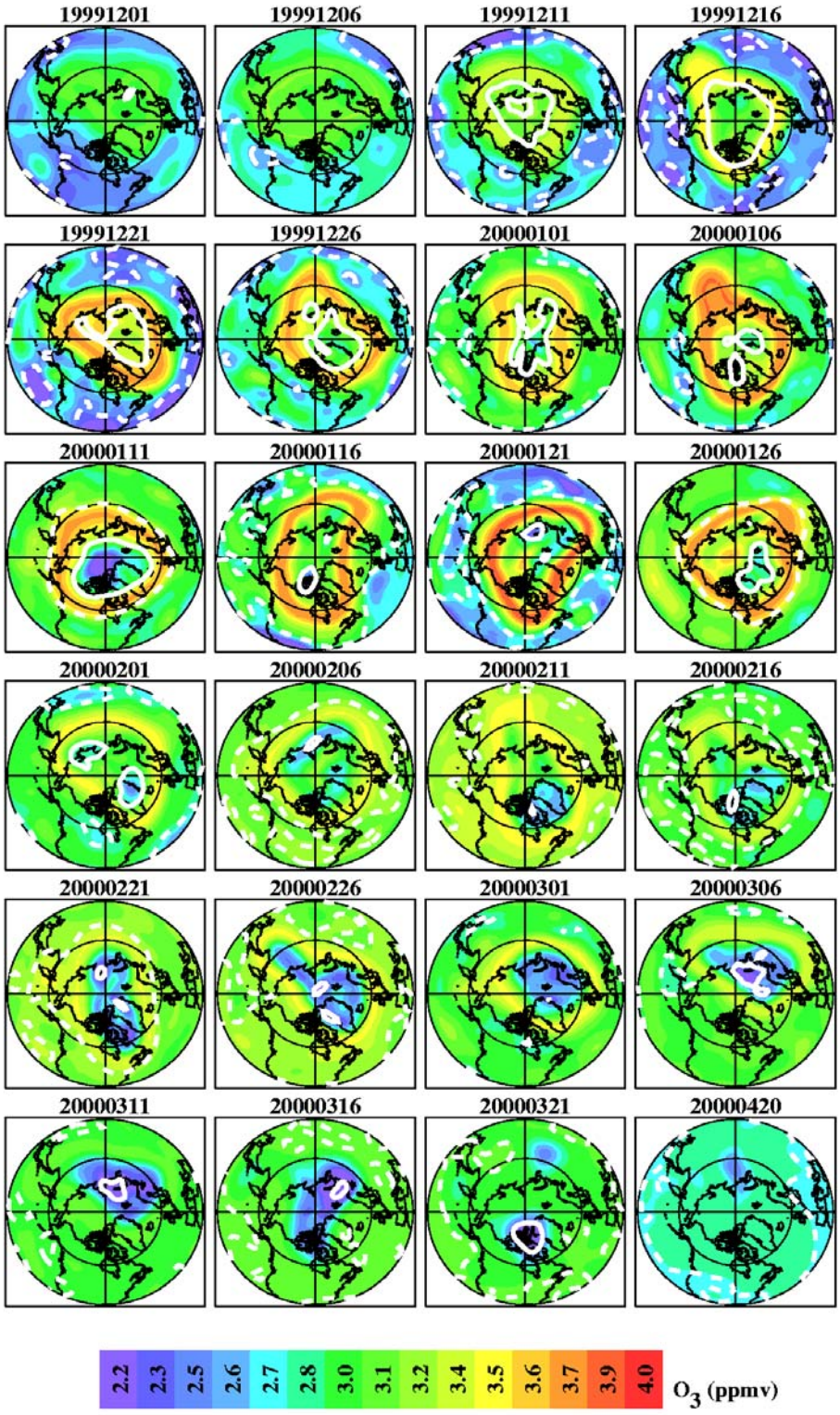

Plate 12. Proxy O_3 maps on the 500 K potential temperature level, as in Plate 6, for the dates shown in each panel. Note that the final panel succeeds the previous one by one month.

Table 1. Ozonesonde stations used in the statistical validation analysis. The number of comparisons from each station that were included in the results shown in Plate 8 is listed in the last column. Profiles were obtained between 22 November 1999 and 1 February 2000.

Station	Latitude	Longitude	# Comparisons
Aberystwyth	52.40	-4.10	5
Alert	82.50	-62.3	8
Andoya	69.30	16.11	6
Churchill	58.74	-94.00	6
De Bilt	52.10	5.18	7
Stonyplain	53.55	-114.	5
Eureka	79.99	-85.9	17
Gardermoen	60.11	11.04	3
Goose Bay	53.18	-60.2	4
Hohenpeissenberg	47.80	11.00	27
Izana	28.46	-16.2	2
Jaegersborg	55.77	12.53	1
Jokioinen	60.80	23.50	12
Lerwick	60.13	-1.18	22
Lindenberg	52.13	14.07	6
Legionowo	52.40	20.97	15
Ny Ålesund	78.93	11.95	29
Orland	63.42	9.24	14
Payerne	46.80	6.95	30
Prague	50.02	14.45	12
Keflavik	63.97	-22.60	4
Resolute	74.71	-94.90	12
Salekhard	66.70	66.70	10
Scoresbysund	70.50	-22.00	10
Sodankyla	67.39	26.65	19
Thule	76.53	-68.70	5
Uccle	50.80	4.35	23
Valentia	51.93	-10.20	6
Yakutsk	62.03	129.60	5
		Total:	325